Design and implementation of smart observable system of indoor hydroponic

N.M. Shah, K.A. Mohd Annuar*, M.H. Harun, M.F. Mohd Abdul Halim, A.H. Azahar

Fakulti Teknologi Kejuruteraan, Universiti Teknikal Malaysia Melaka, Hang Tuah Jaya, 76100 Durian Tunggal, Melaka, Malaysia

*Corresponding e-mail: khalilazha@utem.edu.my

Keywords: Indoor hydroponic; pH sensor

ABSTRACT – As to highlights the pursuit of modernity of a country and living standard of the citizens, everything has to be put up to a standard for a product to be potentially up to date. Hydroponic cultivation is a great way to grow plant to their full potentials. Land has been discovered to build buildings and housing area this cause less land to do plantation. The objective is to establish a smart system that can operate indoor hydroponic for home use, to design the whole electrical system that will combine with hydroponic structure and monitor the pH of the crop and to prove how this system helps in development of better system in agriculture. Two types of soluble fertilizer help in gaining suitable Potential Hydrogen (pH) value. As to accomplish the objectives, users need tools to communicate with whole system and helps in nourishing the plants day by day.

1. INTRODUCTION

The main idea of implementing indoor hydroponic is to conserve our forest. In this study, recycle material was chosen as a main material to build one complete system of indoor hydroponic. Hydroponic allows plants to be grown in a completely controlled environment, soil-barns-pests-free and free from diseases as well. Delicious product can be obtained by careful monitoring the nutrients, temperature, lights level and nutrient water level or solutions level without using dangerous herbicides and pesticides. For that reason, hydroponic gardening is gaining popularity for both commercial and home gardening application all around the world.

According to James Loomis at el., basically ebb and flow is where a nutrient with rich solution flooded into a grow tray containing the plants and roots periodically. The solution then drains back out into the main tank or reservoir [1]. In 2013, Harley N. Smith explained, in order to insure optimal utilization by the plant, pH measurement for both acidity and alkalinity of nutrient solution should be monitored daily [2]. pH is basically a measurement unit of alkalinity and acidity of the nutrient solution which make pH of 7 is neutral, less than 7 is acidic and over than 7 is alkaline or basic. While actually, the most suitable pH reading for better nutrient is between 5.8 to 6.4, or slightly acidic [3]. This is to avoid iron and some others metal elements might be unavailable to the plant and if it is too low, the take-up calcium, magnesium and other macro-element may be hindered.

One thing need to be considered is that an excessive water level in a hydroponic system gain from the rain water or water that gets into the reservoir through outside must be deal with overflow prevention. To solve this problem, drain holes at the higher level of the reservoir allow any excess water to escape without ruining the electronic devices or the plants [4-5].

This paper studies the design of smart observable system of indoor hydroponic. This system involves the implementation of the basic communication between android application with pH level measurement, temperature measurement, level measurement, ventilation system and lighting system.

2. METHODOLOGY

The main concept of this project is to use Bluetooth features in an android phone to control the grow lamp, fan, pump in/out water and nutrient into the tank. The cellphone will be the tool to do all of these discipline including figure out the temperature of the plant. Basically, the temperature sensor will send input data of the current temperature in degrees to Arduino and then Arduino will transfer the data to cellphone with the help of Bluetooth module. The programming of the Arduino is burn by using Arduino IDE Programmer editor and transferred using USB cable from the computer board.

2.1 Framework of the hardware

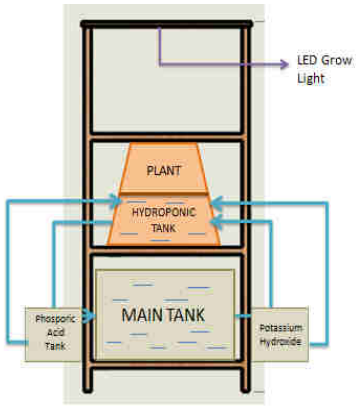

Figure 1 Project flow

Table 1 Type of plant and pH

Plant	pH range
Tomatoes	6.1 – 6.3
Cucumbers	5.6 – 6.5
Spinach	6.1 – 6.4
Lettuce	6.1 – 6.3
Broccoli	6.4 – 7.1

Table 1 shows the type of plant and the pH range needed. This is important, because different plants need different needs of solution to add to so that the plant's pH will balance and it can grow healthily.

3. RESULT AND DISCUSSION

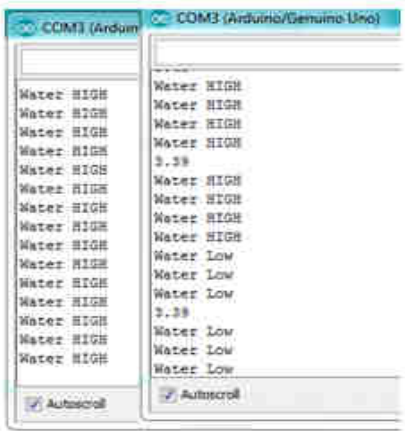

Figure 2 Hardware test result for float switch, water pump and pH sensor

Figure 2 shows the test result for float switch with water pump, which the result shown "water HIGH" indicates the float switch is in "ON" condition showing that water level is at rise, therefore water pump is off. While, another test result shows that pH value with slightly acidic with a value of 3.39 and water is at rise and water pump is off and low simultaneously according to the test.

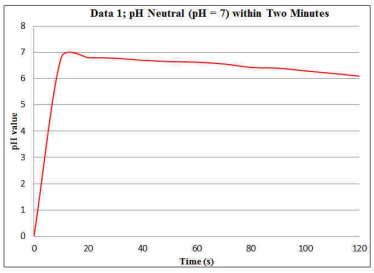

Figure 3 Calibration of pH sensor

At room temperature, the pH of pure water is very close to 7. This condition is considered to be neutral. It is neither an acid nor a base, but is the reference point for acids and bases. The chemical formula for water contains charged hydrogen ion that is bonded to a negatively charged hydroxide ion. This means, water has properties of both acids and bases. Where the properties essentially cancel each other"s out. As time increase, temperature also decrease and hydrogen ion tend to lose, therefore pH value 7 tend to decrease to acidic (Figure 3).

4. CONCLUSIONS

Indoor hydroponic system is a very conducive home furnishing that many people have put eyes on and starting to show some interest at. It is complete with technology or electrical system that brings the comforts of having a growing plant inside or outside of your home. Even there is much different within the developed technology of hydroponic nowadays, hydroponic still promise to provide a better, bigger and healthier yield or crops. The better technology such as sensors and components that helps in regulates the air and acts as an artificial sunlight for the plants, the better and healthier the plant will grow.

ACKNOWLEDGEMENT

The authors would like to thanks for the support given to this research by Ministry of Higher Education Malaysia and Universiti Teknikal Malaysia Melaka (UTeM).

REFERENCES

[1] J. Loomis, K.A. Charif, J. Walker, and M. DiLeonardo, "Leaf Alone Hydroponic System", University of Central Florida, 2014.

[2] H.N. Smith, "Introduction to Hydroponic- Seed to Harvest", pp. 1-15, 2013.

[3] M. Stefan, "The Hydroponic System – A Way to Get Vegetable Crops Through Performance Methods", *Journal of Faculty of Agro-Food and Environment Economics*, pp. 1-5, 2014.

[4] K.A.M. Annuar, N.A.A. Hadi, I.M. Saadon, and M.H. Harun, "Design and Construction of Liquid Level Measurement System", *Journal of Advanced Research in Applied Mechanics*, vol. 12, no. 1, pp 8-15, 2015.

[5] M.F. Saaid, N.A.M. Yahya, M.Z.H. Noor, and M.S.A. Megat Ali (2013), "A Development of an Automatic Microcontroller System for Deep Water Culture (DWC)", in *IEEE 9th International Colloquium on Signal Processing and its Applications*, 2013, pp. 328-332.

Proceedings of Innovative Research and Industrial Dialogue'16, pp. 23-24 (May 2017)

Development of mould for self fabricated ceramic cutting tools

T. Norfauzi[2,*], A.B. Hadzley[1], U.A.A. Azlan[2], M.R.M. Razly[1], M. Hairizal[2]

[1)]Precision Machining Group, Advanced Manufacturing Centre, Faculty of Manufacturing Engineering, Universiti Teknikal Malaysia Melaka, Hang Tuah Jaya, 76100 Durian Tunggal, Melaka, Malaysia

[2)]Faculty of Engineering Technology, Universiti Teknikal Malaysia Melaka (UTeM), Hang Tuah Jaya, 76100 Durian Tunggal, Melaka, Malaysia

[*]Corresponding e-mail: norfauzi@utem.edu.my

Keywords: Mould, ceramic cutting tool, machining

ABSTRACT – This paper introduces the development of mould for fabrication of ceramic cutting tool. The mould that produced involved with main parts divided by the core, cavity and ejector. To produce the mould, cylindrical shape of carbon steel was machined according to the required dimensions, assisted by the CADCAM software. Alumina-zirconia based powders were then processed and inserted into the designated mould in order to evaluate the accuracy and functionality of the mould. The results show that the mould capable to fabricate the green compact of the alumina-zirconia powder with 13% offset of thermal shrinkage. Further test of the sintered alumina-zirconia insert demonstrated the capability of the mould to produce the self-fabricated ceramic cutting tool for the machining operation.

1. INTRODUCTION

Cutting tools can be considered major industrial necessities as it applied mostly in parts production. In machining process, there have many classes of the cutting tools according to the shape such as rectangular, square and round as well as nose radius such as straight, bent, cranked and round-nosed cutter. The shape of the cutting tools was designed depended on the specific condition, such as the material of the tools, the materials that need to be cut and the process conditions [1].

Among many cutting tools available in industry, ceramic is one of the cutting tools that offers high wear resistance and able to be operated at dry condition. Ceramic cutting tools were made by powder processing technique such as powder mixture, pressing and sintering at a suitable temperature. Powders that suitable to be applied as cutting tools including alumina, zirconia, silicon carbide, sialon etc [1].

In order to produce ceramic powder based cutting tools, a special mould is required to compact to powders to from a green body. A simple mould should consist of core, cavity and injector. Core and cavity play important role in ensuring that the mould capability to be inserted, pressed and compacted while the ejector functioned to press away the compacted powders from the mould to form a green body. Misalignment between core, cavity and ejector would create troubles such as product stuck, deformed, tight and crash during part ejection process [2].

This extended abstract present the development of simple mould that built for fabrication of ceramic cutting tool. The core, cavity and ejector of the mould were fabricated by machining cylindrical shape of carbon steel assisted by CNC turning, CNC milling and EDM wire cut. The accuracy of the mould was evaluated based on the accuracy of the ceramic cutting tool, before and after sintering. This study will help to understand rate interest of shrinkage when a ceramic sintering process, mould tolerance and synchronization between core, cavity and ejector when forming ceramic cutting tool.

2. METHODOLOGY

2.1 Material and cutting tool preparation

A cylindrical bar of carbon steel with 36 mm diameter was prepared as the material for a mould development. The cylindrical carbon steel can be shown in Fig. 1. CATIA V5 R23 was used software as a medium to sketch, analysis the mould. This includes the assembly between core, cavity and ejector.

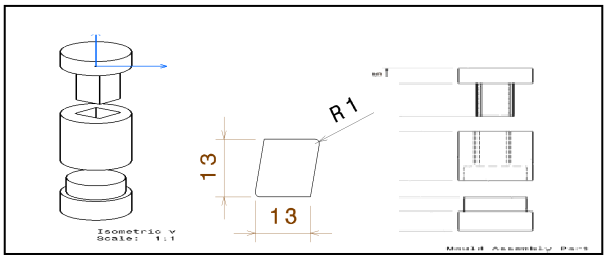

Figure 1 Design by CATIA V5 R23 software

.

2.2 Machining

In order to produce core and the ejector of the mould, CATIA V5 software was used to design and develop a CNC program to machine carbon steel according to the designated shape. On the other hand, EDM Wire Cut was used to create a hole for cavity according to the size of the cutting tool, with consideration of thermal shrinkage after sintering. Figure 2 shows the EDM wire cut and CNC Milling operations to produce the mould.

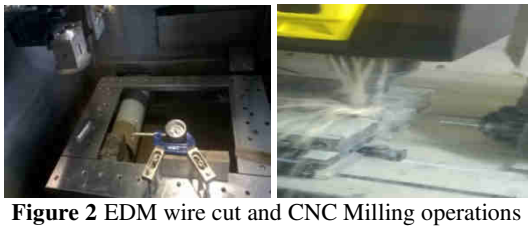

Figure 2 EDM wire cut and CNC Milling operations

It should be noted that the surface of these core, cavity and ejector should be as fine as possible to facilitate smooth movement during product ejecting. This is to prevent sticking between core surface and ceramic powder which can resulting ceramic powder burst. Therefore, the surface of these parts was polished using sand paper to refine their surface finish quality. Fig. 3 shows a comparison of part surfaces before and after polishing process.

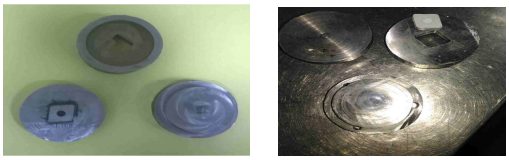

Figure 3 (a) Before polish and (b) After polish

2.3 Powder Processing

Specific composition of alumina-zirconia powders were mixed by a ball mill machine with the addition of polyethylene glycol (PEG) as a binder. Details processing technique can be found in [3]. These homogen powders were inserted into mould cavity and compacted by hydraulic press to produce a green body of ceramic cutting tool. The green body was ejected by using ejector before sintered in the furnace to produce an early sample of the ceramic cutting tool.

3. RESULTS AND DISCUSSION

Fig. 4 (a) shows the core of the mould which designed according to commercial cutting tool design. The function of mould core is to form and press the ceramic powders by using a hydraulic press machine. The core was designed to assist 5 tons pressure to the ceramic powder compacts inside the cavity. The core also designed with adequate tolerance, so it can be penetrated and retracted without any disturbed grip between cavity. Fig. 4(b) shows the cavity of the mould which represented by the hollow shape of the mould. The cavity was designed based on the shape of the cutting tool and the size of the cavity should consider the shrinking size of ceramic powders. Fig. 4(c) shows the ejector part of the mould which located at the back part of the cavity. The function of the mould ejector is to pull out the part with without any pressure so the green compact can be removed easily without any fracture. Mould ejector takes a role to eject the ceramic part from the lower direction of the mould.

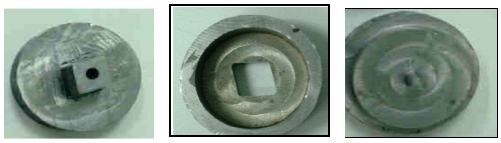

(a) (b) (c)

Figure 4 (a) core (b) cavity and (c) Ejector

Fig. 5(a) shows the commercial cutting tool, green body of ceramic cutting and ceramic cutting tool after sintering. It can be estimated that the mould demonstrated 13% size offset as compared to the shrinkage size of cutting tools compact. In order to evaluate the functionality of the mould, the sintered ceramic was further clamped inside tool holder a shown in Fig. 5 (b). It shows that the cutting tool fit adequately within the tool holder, which shows that the mould developed in this study are suitable for ceramic insert manufacturing. Further experimental test to evaluate the performance of sintered cutting tools produced by this mould will be held in the upcoming trials in the future.

(a) (b)

Figure 5 (a) Ceramic tools and attaches at (b) tool holder in CNC turning

4. CONCLUSIONS

A mould for ceramic cutting tool manufacturing was prepared. The simple mould was designed based on the commercial size of cutting tool which involved with core, cavity and ejector assembly. The process involved was turning, milling, EDM wire cut and polishing. The mould capable to compact and eject the cutting tool powder without sticking and fracture. The thermal offset after sintering recorded at 13%. The ceramic insert prepared from the mould comfortably fit with the tool holder.

ACKNOWLEDGEMENT

The authors are grateful to Universiti Teknikal Malaysia Melaka for serving a platform to perform this study.

REFERENCES

[1] G. Schneider, *Cutting Tool Applications,* ASM International; 2002

[2] A. B. Mohd Hadzley, R. Izamshah, M. Amran, W. Azahar, "Development of Jig for Sintering Hollow Tube Mat", *Applied Mechanics and Materials*, Vol. 761, pp. 631-635, 2015.

[3] A. Z. A. Azhar, L. C. Choong, H. Mohamad, M. M. Ratnam, and Z. A. Ahmad, "Effects of Cr2O3 addition on the mechanical properties, microstructure and wear performance of zirconia-toughened-alumina (ZTA) cutting inserts," *Journal of Alloys and Compounds*, vol. 513, no. 5, pp. 91–96, 2012.

Investigation on the effect of machining strategies on the dimensional accuracy of five-axis flank machining of curvy angled shapes (convex)

M.R.M. Razly[1,*], S.A. Suandi[1], R. Izamshah[1], T. Norfauzi[2]

[1)] Precision Machining Group, Advanced Manufacturing Centre, Faculty of Manufacturing Engineering, Universiti Teknikal Malaysia Melaka, Hang Tuah Jaya, 76100 Durian Tunggal, Melaka, Malaysia

[2)] Faculty of Engineering Technology, Universiti Teknikal Malaysia Melaka (UTeM), Hang Tuah Jaya, 76100 Durian Tunggal, Melaka, Malaysia

[*]Corresponding e-mail: razlyraffay@gmail.com

Keywords: Flank milling, 5-axis machining, dimensional accuracy

ABSTRACT – Over the years, CAM software assist a lot in CAM programming. Various kinds of cutting strategies are served by CAM software. As a user for CAM software, it is preferable to maximize the abilities of CAM software. A little part of problems in CAM programming was identified which is multi axis flank milling. The major problem in flank milling is the cutting strategy. As the consequences, users hardly select the best machining strategy for the certain shape. In fact, it may lead to unsatisfied machining results. Thus, this study initiated to investigate the effect of machining strategies by focusing on curvy angled shape utilizing multi axis flank milling. 5-axis CNC milling machine has been utilized to perform physical machining. The response variables for this study were Tanto Fan, Combin Tanto, and Combin Parelm. As the outputs of this study, Tanto Fan indicated the most accurate dimensional tolerance following by Combin Parelm, and Combin Tanto. The result was discussed and analysed in this study. The tool path generated for all flank strategies are different although the guide and drive (grazing surface) are same. This finding proved that flank cutting tool path contributes towards dimensional accuracy.

1. INTRODUCTION

There are numerous of researches focusing on machining strategies but unfortunately hardly found in flank milling strategies. Yet, very few studies were focusing on the end result of machined sample. In CATIA V5R21, there is a feature called Multi-Axis Flank Milling. However, the strategy provided by CATIA V5R21 are hardly to differentiate since they have many types of strategies and almost same tool path. Figure 1 shows the diagram of each of strategy given by CATIA V5R21. Thus, the main aim of this research is to identify the best machining strategy on the five-axis flank machining curvy angled shapes using various machining approaches or strategies offered by CATIA V5R21 named as Tanto Fan, Combin Tanto, and Combin Parelm.

Figure 1 Toolpath different given by CATIA V5R21

The most crucial part in multi axis flank milling is how to position the tool axis along the grazing surfaces. Hence, applying the right and the best machining strategy in Computer Aided Manufacturing (CAM) process is the most vital phase. Recent research found related to the flank milling machining was reported by Ramy F. Harik et al [1]. They agreed that the flank milling is very important in machining of aircraft structural parts, turbines, blades and several other mechanical parts. A study carried out by Ahmadi et al [2] which is related to the flank milling was about finding out the effect of chattering in flank milling machining. A dynamic model was developed to study the chatter in the flank milling of curved surfaces on a five-axis machining. Even though a lot of research are focusing on flank milling, but still least research focusing on common machining approach which emphasized in CAM programming. Thus, this research approaches will essentially ideal by most of CAM users including industry because of minimal effort, short set up, and straightforward execution. Details mathematical modelling and add-on things would take more efforts in order to obtain better flank cutting results.

2. METHODOLOGY

The research begins with findings actual part modeling. The Endcap shown in Figure 2 suitable and meets the requirement of curvy convex (positive) shapes as this research has been proposed. A few modifications on part model was done by creating stock and rescaled.

CAM programming took into placed after the modification of part. Post processing was the following step to be done once the CAM programming completed. 5-axis CNC milling machine, Deckel Maho DMU 60 Monoblock was utilized for machining process. A series of data generated from the Coordinate Measuring Machine(CMM) was obtained from this experiment.

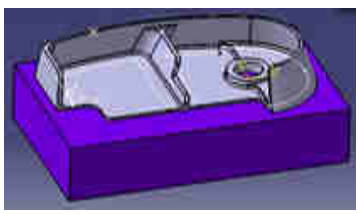

Figure 2 Endcap 3D modeling

3. RESULTS AND DISCUSSION

Data of dimensional accuracy was obtained and catagorized by A, B, and C as shown in the Figure 3. A, B, and C was catagorized because of the axial depth of cut was set to 3 layers. Significantly, these data represent the output and character of Tanto Fan, Combin Tanto, and Combin Parelm. The data was tabulated in the Figure 4. The data in Figure 4 shows that the tool path movement is the most crucial part in order to achieve accurate flank milling [3]. The differences between the response variable are the way cutter approach and moving out by respect to guide and drive (grazing surface).

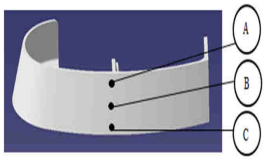

Figure 3 A,B, and C represent each level of measurement

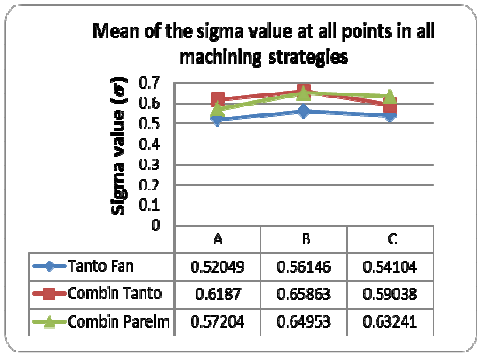

Figure 4 Sigma value for A, B, and C level

Table 1 Rank of dimensional accuracy

Rank	Machining strategies	Mean (σ)
1st	Tanto Fan	0.54100
2nd	Combin Parelm	0.61799
3rd	Combin Tanto	0.62257

From the Table 1, the acquisition of dimensional accuracy rank was tabulated. A finding on the effect of tool path was found in this study. There are three types of basic flank cutting path as shown in figure 5.

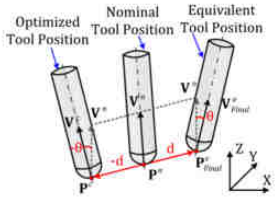

Figure 5 Cutting position in flank cutting

From the illustration in Figure 5, it can be related to flank strategies cutting path. Tanto Fan move as nominal position while Combin Parelm move as optimized tool position and equivalent tool position for Combin Tanto. These behavior of tool position was seen clearly in CAM simulation. Different tool position resulted difference amount of material removal rate due to the engagement of flute angle and tool position. Others possible factor that contribute much in dimensional error is the physical springback. Physical springback deformation occur during the engagement of part and cutter [4]. Part will tendency more to rebound after the cutter passed. Figure 6 show on how the physical springback occurred during the machining process. Overcut or undercut are vulnerable in this situation.

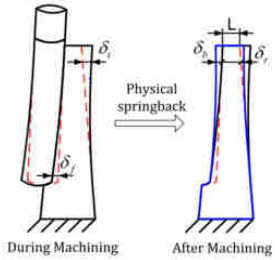

Figure 6 Physical springback effect

4. CONCLUSIONS

The ultimate finding in this study highlighted that Tanto Fan resulted the best dimensional accuracy result of part for the selected sample. This is believed due to the trajectory of tool axis while performing the flank contouring is different from the others strategies parameters. Combin Parelm tool axis is tangent to the drive surface at the specified contact height and follows the curve line isoparametric of the surface smoothly. Combin Tanto tool axis is slightly different from Combin Parelm. Combin Tanto contained in a normal plane to forward direction.

As the impact of this study, CAM programmers are ease in selecting the suitable parameters while performing the CAM programming. Furthermore, this study also contributes to enhance the normal practice in industry that have to run several test cut in order to obtain and fulfil the requirement of specification.

ACKNOWLEDGEMENT

Authors are grateful to Universiti Teknikal Malaysia Melaka for serving a platform to perform this study.

REFERENCES

[1] R. F. Harik, H. Gong, and A. Bernard, "5-axis flank milling: A state-of-the-art review," *CAD Comput. Aided Des.*, vol. 45, no. 3, pp. 796–808, 2013.

[2] K. Ahmadi and F. Ismail, "Machining chatter in flank milling," *Int. J. Mach. Tools Manuf.*, vol. 50, no. 1, pp. 75–85, 2010.

[3] C. Menzel, S. Bedi, and S. Mann, "Triple tangent flank milling of ruled surfaces," *CAD Comput. Aided Des.*, vol. 36, no. 3, pp. 289–296, 2004.

[4] N. Huang, Q. Bi, Y. Wang, and C. Sun, "5-Axis adaptive flank milling of flexible thin-walled parts based on the on-machine measurement," *Int. J. Mach. Tools Manuf.*, vol. 84, pp. 1–8, 2014.

Analysis of KNN films deposited with different annealing temperature

M.A. Mohd Hatta[1,*], M.W. Abd Rashid [1], U.A.A. Haji Azlan[2], N.A.Azmi[1]

[1)] Faculty of Manufacturing Engineering, Universiti Teknikal Malaysia Melaka (UTeM), Hang Tuah Jaya, 76100 Durian Tunggal, Melaka, Malaysia

[2)] Faculty of Engineering Technology, Universiti Teknikal Malaysia Melaka (UTeM), Hang Tuah Jaya, 76100 Durian Tunggal, Melaka, Malaysia

[*]Corresponding e-mail: maziatiakmal@iium.edu.my

Keywords: KNN, annealing, sol-gel

ABSTRACT – This work reports the effects of annealing temperature on the phase formation and crystallographic orientation of KNN films prepared by sol-gel method. The films were annealed in the temperature range of 600-700 ºC and the properties were studied by XRD, FESEM, and EDS-microXRF. The film annealed at 650 ºC exhibits orthorhombic perovskite structure with preferable orientation at (001). It also had homogeneous grains with K, Na, Nb and O atomic elements were detected by EDS-microXRF.

1. INTRODUCTION

Potassium sodium niobate (KNN) thin films tremendously becoming popular for piezoelectric applications due to high Curie temperature (420 ºC), high remnant polarization (14 μC/cm^2) and high piezoelectric constant (~300 pC/N) [1-2]. Numerous methods have been adopted to produce KNN thin films include sputtering [3], pulsed laser deposition [4] and sol-gel methods [5]. Among all techniques, the sol-gel technique is the simplest and economical route to deposit KNN films with homogenous morphology over a large area of the substrate [6]. Though, the sol-gel technique requires proper selection of heat treatment temperature for obtaining the films with good crystallization and uniform morphology which further can improve the piezoelectric properties of the films.

The effect of annealing temperature on the structural, optical and piezoelectric properties of KNN films prepared by other methods have been extensively studied while less research has been dedicated to identify the properties of sol-gel derived KNN films [7]. Therefore, the effect of heat treatment temperature on the structural properties of KNN films prepared by the sol-gel method has been investigated at 600-700 ºC in this work.

2. EXPERIMENTAL

Three stages were involved in fabricating KNN thin films comprise of solution preparation, coating, and annealing. KNN sol was prepared by dissolving sodium acetate (Alfa Aesar, 99% purity), potassium acetate (Alfa Aesar, 99% purity) and niobium ethoxide ($Nb_2OC_2H_5$) in an organic solvent of 2-methyoxyethanol (Sigma-Aldrich, 99.9% purity) with vigorous stirring for 1.5 hours. The sol was then spun onto the Si substrate at 3000 rpm for 60 seconds to produce the thin films. After deposition, the films were pyrolyzed at 200 ºC. Further, the thin films were annealed in the rapid thermal annealing furnace (RTP-1000D4, MTI) at temperature of 600-700 º C.

The phase formation and crystallographic orientation were identified by X-ray diffraction (XRD) using PANalaytic X'Pert Pro from scanning range of 20º to 70º with CuKα radiation. The morphology of annealed film was examined by focused ion beam (FIB, FEI Technai) operating at 30 kV. The elemental analysis was performed using Bruker EDS-microXRF detector.

3. RESULTS AND DISCUSSION

Figure 1 depicts XRD spectra of the synthesized KNN films grown at the different annealing temperature. At 600 ºC and 650 ºC, six prominent peaks were identified indicating that the films are produced with orthorhombic perovskite structure which in agreement with ICCD card. With increasing temperature from 600ºC to 650 ºC, the intensity of peak oriented at (001) became high and more intense. This finding elucidates that the crystallinity of KNN film can be improved at 650 ºC. As annealing temperature raised to 700 ºC, the perovskite peaks of KNN were diminished while spurious peaks of $K_4Nb_6O_{17}$ emerged. The evolution of $K_4Nb_6O_{17}$ phase which also known as tungsten bronze phase is due to rapid volatilization of Na element within the KNN compound [8].

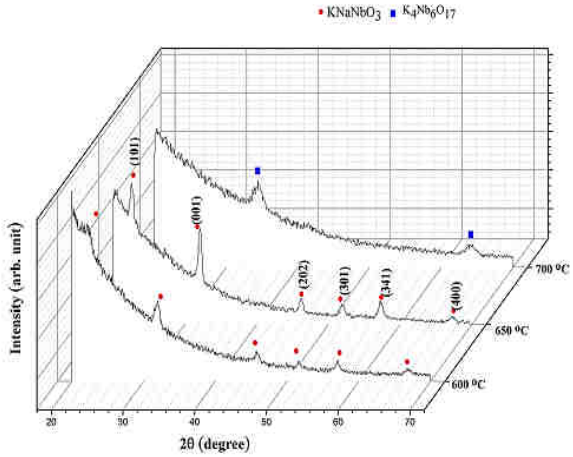

Figure 1 XRD of films annealed at various temperature

Figure 2 demonstrates the morphology of KNN film annealed at 650 ºC. As can be observed, the surface of KNN consists of fine and uniform grains distributed

over the large area of Si substrate. The film was also cracks-free with no trace of secondary phase.

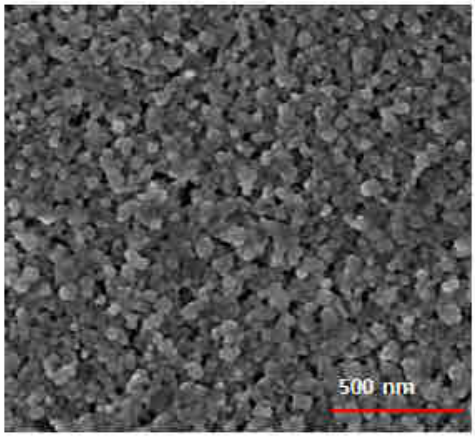

Figure 2 FESEM image of KNN film annealed at 650 °

The complementary EDS-microXRF analysis were performed as shown in Figure 3 to confirm the presence of K, Na, Nb and O elements in KNN compound. EDS spectra represented in purple while microXRF in red spectra. K, Na, Nb and O elements can be easily observed from the intense spectra confirming the presence of host element within KNN compound. Note that; Rh is from X-ray source which also can be detected from this specta.

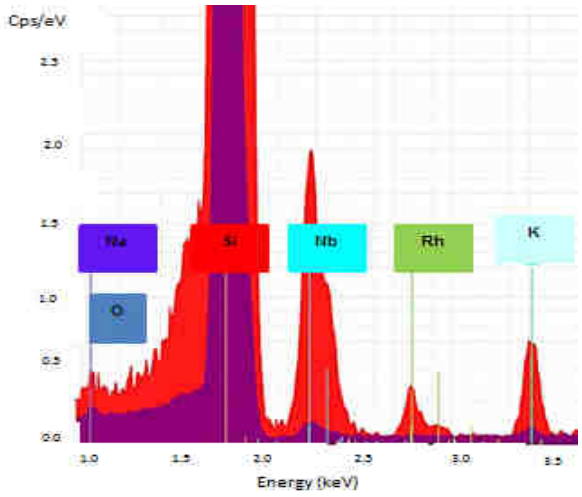

Figure 3 EDS-microXRF spectra of KNN film

4. CONCLUSION

KNN thin films have been deposited using the sol-gel route. KNN films grown at 600 °C and 650 °C shows the pronounce peaks of orthorhombic perovskite phase with film annealed at 650 °C achieved the best crystallization hence being the optimum temperature to grow KNN film. The morphology of KNN grains at optimum temperature was uniform and cracks free. Further, EDS-microXRF confirmed the existence of atomic elements in KNN structure.

ACKNOWLEDGEMENT

The authors are grateful to the Department of Universiti Teknikal Malaysia Melaka (UTeM) and Ministry of Higher Education for funding this research (FRGS/1/2014/TK04/FTK/02/F00207).

REFERENCES

[1] J.Du, J.Wang, G.Zang, and X.Yi, "Phase transition behavior and piezoelectric properties of low-Li and high-Sb modified KNN based piezoceramics," *Phys. B Condens. Matter*, vol. 406, no. 21, pp. 4077–4079, Nov. 2011.

[2] R.Rani, "Influence of Sintering Temperature on Densification, Structure and Microstructure of Li and Sb Co-Modified (K,Na)NbO_3-Based Ceramics," *Mater. Sci. Appl.*, vol. 02, no. 10, pp. 1416–1420, 2011.

[3] T.Li, G.Wang, K.Li, G.Du, Y.Chen, Z.Zhou, and D.Rémiens, "Electrical properties of lead-free KNN fi lms on SRO / STO by RF magnetron sputtering," *Ceram. Int.*, vol. 40, no. 1, pp. 1195–1198, 2014.

[4] M.D.Nguyen, M.Dekkers, E.P.Houwman, H.T.Vu, H.N.Vu, and G.Rijnders, "Lead-free (K0.5Na0.5)NbO3 thin films by pulsed laser deposition driving MEMS-based piezoelectric cantilevers," *Mater. Lett.*, vol. 164, pp. 413–416, 2016.

[5] L.Wang, W.Ren, K.Yao, P.C.Goh, P.Shi, X.Wu, and X.Yao, "Effect of Pyrolysis Temperature on K0.5Na0.5NbO3 Thick Films Derived from Polyvinylpyrrolidone-Modified Chemical Solution," *J. Am. Ceram. Soc.*, vol. 93, no. 11, pp. 3686–3690, Nov. 2010.

[6] A.E.Danks, S.R.Hall, and Z.Schnepp, "The evolution of 'sol–gel' chemistry as a technique for materials synthesis," *RSC Adv.*, vol. 3, pp. 91–112, 2016.

[7] G.Li, X.Wu, W.Ren, and P.Shi, "Effect of excessive K and Na on the dielectric properties of (K,Na)NbO3 thin films," *Thin Solid Films*, vol. 548, pp. 556–559, Dec. 2013.

[8] K.Tanaka, K. Ichi Kakimoto, and H.Ohsato, "Fabrication of highly oriented lead-free (Na, K)NbO3 thin films at low temperature by Sol-Gel process," *J. Cryst. Growth*, vol. 294, no. 2, pp. 209–213, 2006.

Study of cassava based adhesive to reduce warping deformation in 3D printer machine

M.A. Nazan[1,*], F.R. Ramli[1,2], M.R. Alkahari[1,2], M.A. Abdullah[1,2]

[1)] Faculty of Mechanical Engineering, Universiti Teknikal Malaysia Melaka,
Hang Tuah Jaya, 76100 Durian Tunggal, Melaka, Malaysia
[2)] Center for Advanced Research on Energy, Universiti Teknikal Malaysia Melaka,
Hang Tuah Jaya, 76100 Durian Tunggal, Melaka, Malaysia

[*] Corresponding e-mail: muhd_afdhal@hotmail.com

Keywords: Open source 3d printer; warping deformation; tensile test

ABSTRACT – The purpose of this paper is to investigate the used of cassava based adhesive on the platform of 3D printer machines; Kossel Mini, Fab Gear and Mendel Max platform to reduce the warping deformation of PLA printing object. A tensile testing was conducted to measure the strength of the natural based adhesives. In addition, a warping deformation test has been conducted to measure the printing quality of the 3D printer when attached to these adhesives. Based on the results, the cassava with high concentration of borate has better tensile strength with 0.2 kN and maximum elongation of 0.02 mm. Moreover, the Fab Gear open-source 3D printer model resulted in the lowest percentage of warping deformation value compared to Kossel Mini and Mendel Max.

1. INTRODUCTION

Open-source fused deposition modeling is an additive manufacturing that has revolutionized the production of plastic component and has been slowly replacing the conventional subtractive process. However, one of the drawback of the technology is the plastic filament that comes out from it's nozzle tends to shrink and warp also sometimes peeled away from the printing platform. It has been highlighted by several researchers that an adhesive layer between the first layer and printing platform is required to counter the problem [1-2]. Furthermore, Nazan et al. [3] found that a synthetic adhesive can reduce the warping deformation problem by 0.6%.

The purpose of this paper is to investigate the used of cassava flour (CF) based adhesive on the printing platform by using three different types of 3D printer machines; Kossel Mini, Fab Gear and Mendel Max 3D printer model. The stickiness, viscosity and fluid property of cassava adhesive that is combined with hydrochloric acid and sodium borate was investigated. To investigate the strength of the adhesive, several tests such as viscosity test, tensile test and warping deformation test were prepared.

2. METHODOLOGY

Cassava based adhesive was prepared by the substitution of 0.1M of hydrochloride acid and various weights of sodium borate [4]. The hydrochloride acid was pre-heated to 100˚C to mix the cassava flour and sodium borate before the mixture was left to cool at the room temperature. The experiment was repeated by varying different mass of the sodium borate of 0.15g, 0.12g and 0.10g each. Viscosity of each adhesive was measured by using Brookfield viscometer machine with water bath accommodation to obtain the viscosity with different temperature level; 24 ˚C (room temperature), 40 ˚C and 60 ˚C.

Figure 1 Universal material tester machine

Tensile test has been carried out by using Universal Material Tester as shown in Figure 1. This test was based on the Standard Test Method for Tensile Strength of Adhesive by Means Bar and Rod Specimens, ASTM D2095 (reapproved 2015) using the best result from viscous experiment with high viscosity value to determine the tensile strength of the adhesive using bar and rod shaped butt joined specimens. In addition, the test is applicable to measure the adhesive with various adherend materials in either similar or dissimilar combinations.

Furthermore, warping deformation test was prepared by printing a Polylactic Acid (PLA) test samples with rectangular shaped size of 100mm x 30mm x 5 mm by using the three different types of open-source model 3D printer machines. In addition, the printing preferences were set to 13% infill density, 192˚C printing temperature and 0.2mm of printing layer height. The warping deformations of these samples were measured by using Vernier height gauge.

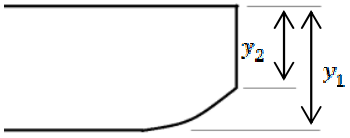

Figure 2 Method of measurement at each sample's corner

$$Waping\ deformation, y = \left|\frac{y_1 - y_2}{y_1}\right| x\ 100\% \quad (1)$$

In Figure 2 and Equation (1), method to measure the warping deformation are presented. By referring to the Eq.(1), the value of percentages of warping deformation is obtained by the difference value of value of total height, y_1 and the deflected total height, y_2.

3. RESULT AND DISCUSSION

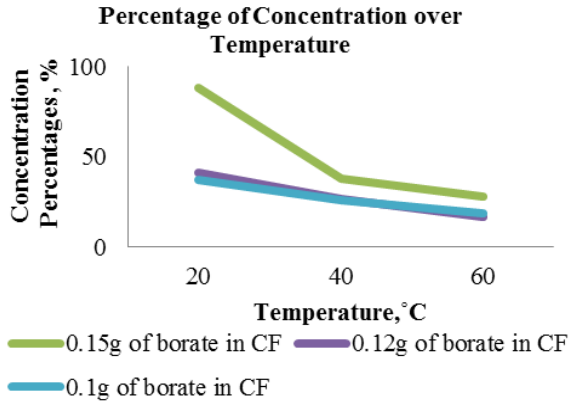

Figure 3 Percentages of concentration over temperature

Figure 3 shows the concentration percentages of the cassava when mixed with the sodium borate and hydrochloric acid over various temperature. The graph shows that the highest percentage of concentration is when 0.15g of sodium borate were added into 50ml of 0.01M HCL and 2.5g of CF with 2129.14 cP of viscosity. This is because the concentration will increase the mass of sodium borate. Thus, the adhesive with 0.15g of sodium borate is chosen for the tensile test.

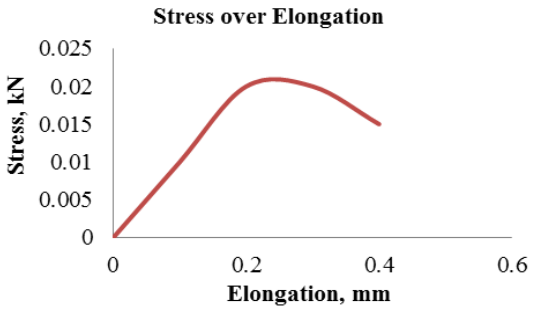

Figure 4 Tensile test on relation of stress applied over displacement

The graph in Figure 4 shows that the peak of the stress using the adhesive mixed with 0.15g of sodium borate is 0.2kN while the displacement is about 0.2mm. This can be interpreted that the adhesive has low elasticity and low elongation value.

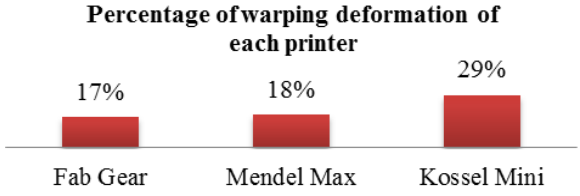

Figure 5 Percentage of Warping Deformation of Each Printer

Figure 5 shows the percentage of warping deformation that occurs for each printer model. Based on the results, the Fab Gear has the lowest deformation value with 17% compared to Kossel Mini and Mendel Max model 3D printer, with 29% and 18%. This is because of the platform surface of fab gear is better prepared and well calibrated compared to the others.

4. CONCLUSIONS

As a conclusion, the borate is proved to gain the adhesive concentration and also improve the properties of the natural based adhesive. The maximum tensile test of cassava based natural adhesive is 0.2kN and the elongation is about 0.02mm. Moreover, the Fab Gear open-source 3D printer model has the lowest percentage of warping deformation value compared to Kossel Mini and Mendel Max.

ACKNOWLEDGEMENT

The authors would like to thank to the Ministry of Higher Education (MOHE), MyBrain15 and Centre for Advanced Research on Energy (CARe), Faculty of Mechanical Engineering (FKM), Universiti Teknikal Malaysia Melaka (UTeM) for sponsoring this research study under the research grant FRGS/1/2015/TK03/FKM/02/F00270.

REFERENCES

[1] W. Z. Wu, P. Geng, J. Zhao, Y. Zhang, D. W. Rosen and H. B. Zhang. "Manufacture and thermal deformation analysis of semicrystalline polymer polyether ether ketone by 3D printing." *Materials Research Innovations,* vol.18, supplement 5, S5-12, 2014.

[2] F. Ramli, M. Jailani, H. Unjar, M. Alkahari and M. Abdullah, "Integrated recycle system concept for low cost 3D-printer sustainability", *Proceeding of Mechanical Engineering Research Day 2015*, 2015, pp. 77-78.

[3] M. Nazan, F. Ramli, M. Alkahari and M. Abdullah, "Optimization of warping deformation in open source 3d printer using response surface method", *Proceeding of Mechanical Engineering Research Day 2016*, 2016, pp. 71-72.

[4] Akhabue, C., Ebewele, R. and Oyedoh, E. "Effects of Preservative Agents on Cassava Starch Adhesives". *AMR*, vol. 62-64, pp 404-411, 2009.

Development of RFID tracking system for wheeled trolleys within an automotive industry

Y.C. Huong[1,*], Z. Jamaludin[1], L. Abdullah[1], R. Haron[2], M.F. Abdullah[2], K.B.A. Jalal[2]

[1)] Faculty of Manufacturing Engineering, Universiti Teknikal Malaysia Melaka, Hang Tuah Jaya, 76100 Durian Tunggal, Melaka, Malaysia

[2)] PHN Industry Sdn Bhd, Jalan Industri 9, Kawasan Perindustrian Alor Gajah, Alor Gajah, 78000 Alor Gajah, Melaka, Malaysia

[*]Corresponding e-mail: yuchung.huong@gmail.com

Keywords: RFID, logistics, returnable transport item (RTI)

ABSTRACT – Asset tracking is one of the focal point of RFID application within manufacturing enterprise, especially for returnable transport item (RTI). The status of RTI is valuable for an enterprise because repeatability use of RTI would eventually reduce asset cost. RFID technology is able to track the status of RTI by obtaining the unique information from RFID transponder tagged on the respective RTI. An RFID system development involves both hardware and software components. However, this paper focuses only on software development of a tracking RTI system that includes a graphical user interface (GUI) and database.

1. INTRODUCTION

Automatic identification and data capture (AIDC) technology is known to improve information flow of logistics. Among AIDC technologies, radio frequency identification device (RFID) is the most promising technology that is able to collect multiple data in real-time without the need for line of sight [1]. RFID is an automatic identification that read and writes unique information through electromagnetic signals. The electromagnetic signals transmitted by RFID interrogator is received by a RFID transponder that is attached on the object. The RFID transponder then responses by sending back unique information of the object.

However, due to high investment cost of RFID technology in item-level [2], most RFID applications are implemented with material handling equipment such as pallet, container, forklift truck and wheeled trolley. RFID is able to perform cost effective scheduling of material handling equipment [3] as exact location of the equipment is known.

Current automotive industry practices outsourcing. Therefore, material handling equipment is always on the move between part supplier and assembler in a closed loop manner, and is known as returnable transport items (RTI) [4]. The automotive parts are delivered either using wheeled trolley that involve low cost, or forklift truck in case of heavy parts.

The value of RFID in RTI management has been proved to be worthy by reducing logistics operation time and cost, as well as reducing the transferral of loss cost [5]. Nevertheless, historically, RFID technology faced difficulty when applied with on-metal application because metal reflects and detunes electromagnetic waves [6]. This difficulty is usually the focal point in the RFID hardware development. This paper presents the software development for tracking of RTI that integrates graphic user interface (GUI) with the RFID system interface. The database applied is based on actual data provided by PHN Industry Sdn. Bhd, Pegoh plant, Melaka.

2. METHODOLOGY

The wheeled trolley tracking system requires software interface to allow communication between user and RFID system hardware. Software development of wheeled trolley tracking system consists of two main parts, which are the GUI and the database. A GUI was developed in a host computer to display the collected information from the RFID system. Several databases are created in order to store information that is required for the application features of the wheeled trolley tracking system.

2.1 Specification of system software

The wheeled trolley tracking system is developed in Window 10 operating system environment. The host computer is installed with net framework 4.5, and Microsoft database engine such as structured query language (SQL) server. Table 1 shows the software used to develop the GUI and the database of wheeled trolley tracking system.

Table 1 Software used in developing tracking system

Program	Software	Reason
GUI	Microsoft Visual Studio 2015 (Community Version)	Provide graphic toolbox options and ease of programming with both C# and visual basic (VB) languages
Database	SQL Server 2014 Management Studio	Ease of learning and wide applications in Windows operating system machine

2.2 System software architecture

The system software consists of three main tiers; (i) user client tier, (ii) application tier, and (iii) data tier. Application tier consists of presentation layer, business logic layer and data access layer. The function of each tier in software development is described in Table 2.

Table 2 Tiers of software tracking system

Tier	Description
Client	To allow user to give command to machine and retrieve stored information from machine and display responses of user command in human language.
Application	To coordinates application, process commands, makes logical decision on the tracking system, as well as process data obtained from database.
Data	To retrieve unique information from RFID transponder through DLL commands and store collected information in data server.

3. RESULTS AND DISCUSSION

The wheeled trolley tracking system was developed based on the architecture shown in Figure 1. The tracking system is applicable using Windows 10 operating system, with at least net framework 3.5 and installed SQLEXPRESS server.

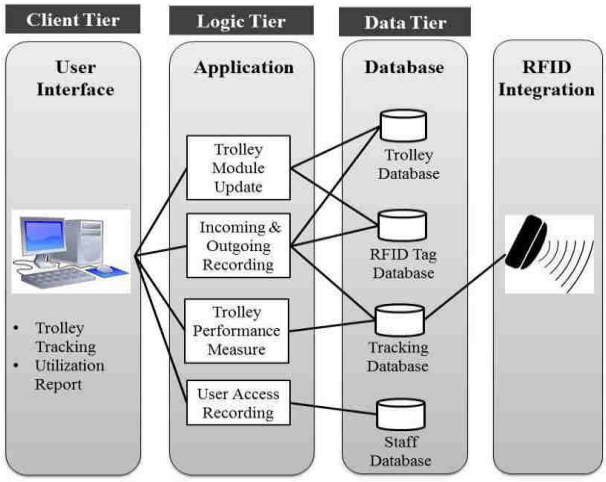

Figure 1 Architecture of wheeled trolley tracking system

The data tier collects the information of wheeled trolley ID number as it travelled within the reading range of the RFID interrogator. Incoming and outgoing recorder then determines the exact status and logistic operation time of the wheeled trolley at the point of RFID interrogator. As a result, a monitoring and tracking system of wheeled trolley is capable to identify the exact location of a wheeled trolley and thus reducing the time previously allocated to determine the where-about of the unit within the assembler facility or part supplier facility.

This system produces dynamic database as data is being collected and updated continuously. These dynamic database in-turns is linked with the static database; such as trolley database and RFID tag database in order to obtain detailed information of the carrying item on the respective wheeled trolley. Detailed information of the wheeled trolley could then assists the logistics operation for inventory control, such as knowing the inventory level of the specific material.

By analyzing the information of incoming and outgoing recorder, performance measure of trolley such as trolley utilization rate, cycle time of trolley in material handling and trolley transferal of loss and damage cost can now be identified.

4. CONCLUSIONS

RFID assisted logistics operations have been encouraged throughout supply chain because it is able to improve logistics performance in term of cost reduction and optimum operation cycle time. RFID system requires both hardware and software integration in order to communicate the machine with the user. Specific for software development, it is essential to have static and dynamic database so that data comparison and analysis can be performed. Hence, RFID software development includes client tier links between user and host machine, application tier make use of rules and database, and data tier store information retrieved from the RFID to host machine.

ACKNOWLEDGEMENT

The authors would like to acknowledge the Ministry of Higher Education Malaysia through University of Science Malaysia for the financial support provided under Knowledge Transfer Programme (KTP), GLUAR/KTP/1/2015/FKP/1//G00038. The authors would also like to appreciate the PHN Industry Sdn. Bhd as partner industry and the Faculty of Manufacturing Engineering, UTeM for the facilities provided.

REFERENCES

[1] X. Fan, "Progress on RFID technology application in logistics industry," in *2010 International Conference of Logistics Engineering and Management*, 2010, pp. 2375-2381.

[2] S. Azevedo, and H. Carvalho, "Contribution of RFID technology to better management of fashion supply chains," *International Journal of Retail & Distribution Management*, vol. 40, no. 2, pp. 128–156, 2012.

[3] V.V. Sople, *Logistics management – the supply chain imperative*, 2nd ed. New Delhi: Pearson Education; 2010.

[4] IC-RTI, 2003. Reusable Transport Items (RTI): Organisational Recommendations. International Council for Reusable Transport Items, German.

[5] A. Ilic, J.W.P. Ng, P. Bowman, and T. Staake, "The value of RFID for RTI management," *Electronics Markets*, vol. 19, no. 2-3, pp. 125–135, 2009.

[6] J. Wagner, R. Fischer, and W.A. Guinthner, "The influence of metal environment on the performance of UHF smart labels in theory, experimental series and practice," in *1st Annual RFID Eurosia*, 2007, pp. 1–6.

Proceedings of Innovative Research and Industrial Dialogue'16, pp. 33-34 (May 2017)

Robust super twisting sliding mode control for machine tools

T. H. Chiew*, Z. Jamaludin*, A.Y. Bani Hashim, L. Abdullah, N.A. Rafan

Advanced Manufacturing Centre, Faculty of Manufacturing Engineering, Universiti Teknikal Malaysia Melaka, Hang Tuah Jaya, 76100 Durian Tunggal, Melaka, Malaysia

*Corresponding e-mail: fosterchiew87@hotmail.com; zamberi@utem.edu.my

Keywords: Machine tools, super twisting, robustness

ABSTRACT – Tracking and robustness are important factors in precise positioning. This paper compares the tracking performance and robustness of super twisting sliding mode controller with traditional controllers on machine tools. The proposed controller was designed and tuned using one factor at a time method, and was experimentally validated on a direct drive single axis positioning system. Its stability was ensured using Lyapunov stability criterion. Results showed the superiority of the proposed algorithm against cascade controller and pseudo sliding mode controller in terms of tracking performance and robustness during load variation. This novelty promotes it as an attractive option for real-time application.

1. INTRODUCTION

The second order sliding mode control (SOSMC) had become one of the favourite methods to engineers and academicians especially in control engineering field to satisfy the high demand on accuracy and precision for machine tools. The main advantage of SOSMC is the superiority in chattering suppression while maintaining its robustness towards parameter uncertainty and high disturbance rejection property [1].

The SOSMC families including twisting, sub-optimal and super twisting algorithms had a wide range of applications which can be found in literature such as marine engineering [2], robotic systems [3] as well as power system [4]. Yet, there are still lacking of experimental validation on robustness of SOSMC in literature especially for the application of super twisting sliding mode control (ST-SMC) in machine tools. Thus, the aim of this paper is to provide a comparison between the tracking responses and robustness of the system controlled with ST-SMC and different controllers. Improvement of tracking performance on single axis positioning system using ST-SMC was also demonstrated experimentally.

2. METHODOLOGY

2.1 System identification

Figure 1 shows the configuration of the overall experimental setup. A single-input-single-output (SISO) model was used to describe the dynamics of the single axis positioning system using frequency domain identification method. A band-limited white noise signal was used as the excitation signal at sampling frequency of 5000 Hz. The SISO frequency response function (FRF) was estimated based on measured output position and input voltage using H1 estimator. The second order transfer function, $G(s)$ and its time domain representation were shown in (1) and (2) respectively.

$$G(s)=\frac{Y(s)}{U(s)}=\frac{A}{s(s+B)}e^{-sT_d} \tag{1}$$

$$\ddot{y}(t)=-B\dot{y}(t)+Au(t) \tag{2}$$

where A = 7.5×10^8 μm/Vs^2, B = 3622 s^{-1} and T_d = 0.00045 s. $Y(s)$ and $U(s)$ represent the actual output position in micrometer and input voltage in volt, respectively.

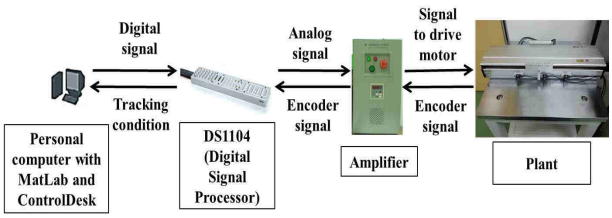

Figure 1 The overall experimental setup

2.2 Design of super twisting algorithm

Two main components, namely; sliding surface, $s(t)$ and control laws were considered in designing ST-SMC. The general formulae for the sliding surface that relates the tracking error, $e(t)$ and first time derivative of tracking error, $\dot{e}(t)$ with a positive constant, λ were shown in (3).

$$s(t)=\left(\lambda+\frac{d}{dt}\right)^{n-1}e(t);\quad e(t)=y(t)-r(t) \tag{3}$$

where n, $y(t)$ and $r(t)$ indicate the order of the uncontrolled system, output position, and desired position respectively. On the other hand, the control law of ST-SMC comprises three components, namely; the equivalent control, $u_{eq}(t)$, that includes a feedforward of velocity and acceleration, the continuous state function, and the discontinuous input, $u_1(t)$ with integrator as shown in (4) and (5). The $u_{eq}(t)$ was obtained using derivation and substitution when $s(t)$ = 0 and $\dot{s}(t)$ = 0 as shown in (6).

$$u(t)=u_{eq}(t)-L\left|s(t)\right|^{0.5}sign\,(s(t))+u_1(t) \tag{4}$$

$$\dot{u}_1(t)=-Wsign\,(s(t)) \tag{5}$$

$$u_{eq}(t)=\frac{1}{A}(\dddot{r}(t)+B\ddot{y}(t)-\lambda\dot{e}(t)) \tag{6}$$

where both L and W are positive gains. These two gains

were tuned using one factor at a time method, and their respective value is 0.00002 and 0.08. The stability was ensured based on Lyapunov criterion [5]. Figure 2 shows the schematic diagram of the designed control algorithm. A Kalman-Bucy filter was added into the system as estimator for better accuracy.

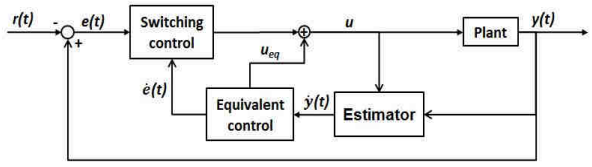

Figure 2 General control scheme for ST-SMC

3. RESULTS AND DISCUSSION

Tracking performance and robustness of ST-SMC were determined in terms of root mean square error (RMSE) and load variation by comparing to a cascade proportional/proportional-integral (P/PI) controller and a pseudo-SMC.

3.1 RMSE

Experiment was conducted by exciting the system using sinusoidal input signal with amplitude 20 mm and frequencies of 0.5 Hz and 1.0 Hz to determine the tracking performance of three controllers when frequency was varied. The RMSE were calculated and tabulated in Table 1.

Table 1 Comparison of RMSE for different frequency

Frequency (Hz)	RMSE (μm)		
	Cascade P/PI	Pseudo-SMC	ST-SMC
0.5	126.6748	2.5942	2.0312
1.0	252.5814	13.7742	4.5817

ST-SMC produced the least RMSE value compared to cascade P/PI and pseudo-SMC. Both pseudo-SMC and ST-SMC produced far better results than cascade P/PI as both are advanced nonlinear controller which are capable in compensating other factors such as parameter uncertainty and noises. Furthermore, the results also showed the consistent performance of ST-SMC when frequency of input signal was varied. Pseudo-SMC produced a large variation in RMSE when the frequency of input was doubled as a tradeoff in reducing chattering effect that usually associated with SMC.

3.2 Load variation

In the next experiment, loads of 0.5 kg and 1.0 kg were introduced into the system for robustness analysis with sinusoidal input signal of amplitude 20 mm and frequency 0.5 Hz. Table 2 presents the RMSE values obtained.

Results from Table 2 showed that ST-SMC produced better robustness compared to cascade P/PI and pseudo-SMC. Great variation in RMSE was observed in the case of 1.0 kg for cascade (0.7457 μm) and pseudo-SMC (0.1994 μm). However, the ST-SMC was still able to maintain its performance (only variation of 0.1507 μm) although heavier load was used. This showed that ST-SMC provided higher robustness for parameter uncertainty compared to cascade and pseudo-SMC.

Table 2 RMSE of different controllers for load variation

Load (kg)	RMSE (μm)		
	Cascade P/PI	Pseudo-SMC	ST-SMC
0	126.6748	2.5942	2.0312
0.5	127.2580	2.6647	2.1087
1.0	127.4205	2.7936	2.1819

4. CONCLUSION

The main contribution of this work is the comparison between cascade P/PI, pseudo-SMC and ST-SMC in terms of tracking performance and robustness on machine tools. Although the robustness is limited to mass variation factor only, this work still showed the improvement of tracking performance and robustness in machine tools through the application of ST-SMC in a single axis positioning system. The results disclosed that the proposed controller was superior against classical controller and pseudo-SMC in terms of tracking error reduction and robustness. For future works, artificial intelligent, e.g. fuzzy logic and neural network can be considered for parameters tuning purpose in ST-SMC.

ACKNOWLEDGEMENT

Authors would like to acknowledge the financial support from Malaysia Ministry of Higher Education through research grant with reference number of FRGS/1/2015/TK03/FKP/02/F00281.

REFERENCES

[1] L. Fridman, J. Moreno, and R. Iriarte, *Sliding mode after the first decade of the 21st century: State of art*, Berlin: Springer Science & Business Media; 2001.

[2] Z.H. Ismail, and V.W.E. Putranti, "Second order sliding mode control scheme for an autonomous underwater vehicle with dynamic region concept," *Mathematical Problems in Engineering*, vol. 2015, pp. 1-13, 2015.

[3] A. Merheb, F. Bateman, and H. Noura, "Passive and active fault tolerant control of octorotor UAV using second order sliding mode control", in *IEEE Conference on Control Applications*, 2015, pp. 1907-1912.

[4] F. Valenciaga, and P.F. Puleston, "High-order sliding mode control for a wind energy conversion system based on a permanent magnet synchronous generator," *IEEE Transactions on Energy Conversion*, vol. 23, pp. 860-867, 2008.

[5] A. Moreno, and M. Osorio, "Strict Lyapunov functions for the super-twisting algorithm," IEEE *Transactions on Automatic Control*, vol. 57, pp. 1035-1040, 2012.

Effects of nanographene addition on tensile and electrical properties of Nylon 6,6 nanocomposites

N. Abdullah Sani[1], M.E. Abd Manaf[1,*], N. Mohamad[1], M.I. Shueb[2]

[1)] Carbon Research Technology, Faculty of Manufacturing Engineering,
Universiti Teknikal Malaysia Melaka, Hang Tuah Jaya, 76100, Durian Tunggal, Melaka, Malaysia

[2)] Radiation Processing Technology Division, Malaysian Nuclear Agency, Bangi, 43000 Kajang, Selangor, Malaysia

[*]Corresponding e-mail: edee@utem.edu.my

Keywords: Nanographene, tensile properties, electrical properties

ABSTRACT – The effects of nanographene (NG) filler on tensile and electrical properties of nylon 6,6 nanocomposite were analyzed. The samples were fabricated by blending nylon 6,6/NG in Sino compounder twin screw machine which subsequently injected into standard size specimens for tensile and electrical conductivity test. An addition of small percentages of NG filler, i.e., 0.3, 0.5 and 1.0 wt% significantly affected the tensile performance and electrical conductivity of nylon 6,6 nanocomposites, in which tensile properties and electric conductivity improved with increasing nanographene filler loading.

1. INTRODUCTION

In recent years, there have been an increasing number of literatures on graphene incorporated polymer composite in pursuit of enhancement on mechanical, thermal and electrical properties. Up to present, graphene is emerging to be a promising material in range of application from construction, transportation, sensors, thermal conductor and electromagnetic interference due to its superior intrinsic properties. Graphene is a new class of monolayer carbon atoms that are arranged into 2D hexagonal pattern and has various advantages [1]. Comparison on mechanical, thermal and electrical properties of graphene has proven its outstanding performance against CNT, steel, Kevlar, HDPE and rubber [2]. Nanographene addition holds the potential to boost electrical conductivity and mechanical by creating electrical path and providing stress transfer advantage in the composite, respectively [3,4]. There have been many studies examining the effects of nanographene filler addition on composites [4-7], however only few studies on nanographene reinforced nylon 6,6 based material have been reported. Hence, the goal of this study is to explore the effects of nanographene addition on tensile and electrical properties of nylon 6,6 nanocomposites.

2. METHODOLOGY

2.1 Materials

Composite samples were fabricated by using nylon 6,6 and nanographene filler at different weight percentage of 0.3, 0.5 and 1.0 wt%. They were both supplied by Terra Techno Engineering. Initially, nanographene and nylon 6,6 were dry-mixed using high speed mixer at 50 rpm to form 3 kg of homogenous mixture which then dehumidified at 70 °C for 3 hours. After that, the mixture was compounded using Sino PSM 30 co-rotating twin screw extruder and crushed into pallet form before injected into standard specimen shape (ASTM D638 Type 4) by using table top injection molding (Ray Ran–Plunger Type).

2.2 Testing

Tensile properties of nylon 6,6/NG nanocomposite were performed in accordance to ASTM D638 using Universal Testing Machine (UTM). The results of tensile strength, Young's modulus and elongation at break were reported. Meanwhile, electrical conductivity test was performed using LCR meter (Agilent Precision LCR meter - E4980A) on disc samples (d = 25 mm), to study the effect of nanographene addition to the electrical conductivity of nylon 6,6/NG nanocomposites.

3. RESULTS AND DISCUSSION

3.1 Tensile properties

Table 1 shows the average results of tensile strength, Young's modulus and elongation (%) at break. The results demonstrate a significant contribution of nanographene filler to the composite, where the tensile strength and Young's modulus increase as nanographene filler increases. Addition of merely 1.0 wt% of nanographenen gives an increase of 5.5% and 10.2% in tensile strength and Young's modulus, respectively. An efficient mixing process that resulted in uniformly dispersed filler contributed to sufficient matrix-filler adhesion, hence improved the material's strength. As the reinforcing material, nanographene provides favorable stress transfer within the composite which leads to higher tensile strength and Young's modulus compared to non-reinforced sample.

Table 1 Tensile properties of nylon 6,6/NG

Sample (NG%)	Tensile Strength (MPa)	Young's Modulus (GPa)	Elongation (%)
NG(0.0)	50.5	1.67	3.46
NG(0.3)	51.8	1.74	1.67
NG(0.5)	52.8	1.76	2.35
NG(1.0)	53.3	1.84	2.59

However, the maximum elongation of composite

decreases as nanographene filler content increases, indicating an increase in stiffness. The result shows that a small amount of NG filler could restrict the molecular mobility of composite, hence decreases its maximum elongation [8]. This is consistent with the increase of Young's Modulus with increasing filler content, indicating more resistance towards elastic deformation. The difference in fracture surface after the addition of 1.0 wt% of NG is shown in Figure 1.

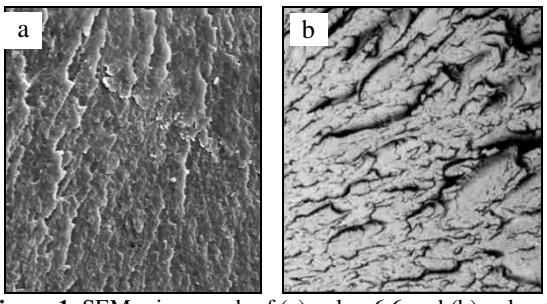

Figure 1 SEM micrograph of (a) nylon 6,6 and (b) nylon 6,6 added with 1.0 wt% NG

3.2 Electrical Conductivity

Figure 2 clearly shows the electrical conductivity of nylon 6,6/NG nanocomposite increases drastically even with a minimal (0.3 wt%) nanographene filler addition. Like most polymers, nylon 6,6 behaves more as electric insulator. But with the presence as little as 0.3 wt% of conductive nanographene filler, its electric conductivity improved significantly due to formation of conductive path by nanographene through the material [3]. As the concentration of conductive filler increases, the filler nanoparticle generates closer contact to each other and spread the electric charge efficiently resulting in higher conductivity as reflected by the result of filler content addition from 0.3 to 1.0 wt%. As reported elsewhere, the electrical conductivity of the nanocomposite is strongly influenced by the synthesis method, type of nanofiller, type of polymer, disantaglement of filler agglomerates and dispersion of nanoparticle [2].

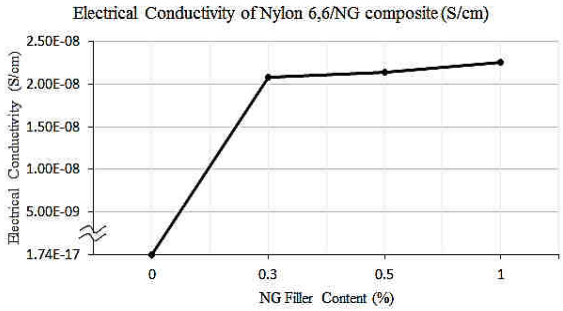

Figure 2 Electrical conductivity versus NG content

4. CONCLUSIONS

The significant effects of nanographene filler to the tensile properties and electrical conductivity of nylon 6,6/NG composite have been observed in this study. Regarding tensile properties, increased content of nanographene filler resulted in higher tensile strength and Young's modulus, but lower % elongation at break of the composite sample. This finding shows that as the filler content increases, the resistance of elastic deformation increase due to restriction of its molecular mobility that creates stiffer material. Meanwhile, the electrical conductivity of the composite shows a linear increase with the addition of nanographene filler due to the conductive charge mobility of nanographene that transfers the charge from one particle to another.

ACKNOWLEDGEMENT

The authors would like to thank the Ministry of Science & Technology (MOSTI) for Science Fund financial support (03-03-01-SF0165). We also thank the Faculty of Manufacturing Engineering of UTeM and Malaysian Nuclear Agency for providing the equipment and technical supports which made this work possible.

REFERENCES

[1] P.Parvin, Z.Ghorannevis, P.Taghdiri, and S. Zahra, "Magnetic measurements of graphene and defected graphene generated by laser ablation method," *Int. J. of Optics and Photonics*, vol. 9, pp. 35-42, 2015.

[2] D.Verma, P.C.Gope, A.Shandilya, and A. Gupta, "Mechanical-thermal-electrical and morphological properties of graphene reinforced polymer composites: A review," *Trans. Indian Inst. Met.*, pp. 803–816, 2014.

[3] K.Sever, I.H.Tavman, Y.Seki, A.Turgut, M. Omastova, and I.Ozdemir, "Electrical and mechanical properties of expanded graphite/high density polyethylene nanocomposites," *Compos. Part B Eng.*, vol. 53, pp. 226–233, 2013.

[4] M.Cano, U.Khan, T.Sainsbury, A.O. Neill, Z. Wang, I.T.Mcgovern, W.K.Maser, A.M. Benito, J.N. Coleman, and E.-Zaragoza, "Improving the mechanical properties of graphene oxide based materials by covalent attachment of polymer chains," *Carbon N. Y.*, vol. 52, pp. 363–371, 2012.

[5] J.Longun and J.O.Iroh, "Nano-graphene/polyimide composites with extremely high rubbery plateau modulus," *Carbon N. Y.*, vol. 50, no. 5, pp. 1823–1832, 2012.

[6] M.Wang, S.Zhang, J.Dong, Y.Song, J.Mao, H.Xie, Y.Qian, Y.Huang, and Z.Jiang, "A Facile route to synthesize nanographene reinforced PBO Composites Fiber via in Situ Polymerization," *Polymers (Basel).*, vol. 8, no. 7, pp. 251, 2016.

[7] M.Chaharmahali, Y.Hamzeh, G.Ebrahimi, A. Ashori, and I.Ghasemi, "Effects of nano-graphene on the physico-mechanical properties of bagasse/polypropylene composites," *Polym. Bull.*, vol. 71, no. 2, pp. 337–349, 2014.

[8] O.A.Al-Hartomy, F.Al-Salamy, A.A.Al-Ghamdi, M.Abdel Fatah, N.Dishovsky, and F.El-Tantawy, "Influence of graphite nanosheets on the structure and properties of PVC-based nanocomposites," *J. Appl. Polym. Sci.*, vol. 120, no. 6, pp. 3628–3634, 2011.

Mechanical properties of kenaf reinforced polypropylene composites added with oil palm shell powder and its activated carbon

M.A.A. Latif [1], M.E.A Manaf [1,*], Z. Shamsudin[2]

[1)] Carbon Research Technology Research Group, Advanced Manufacturing Centre, Faculty of Manufacturing Engineering, Universiti Teknikal Malaysia Melaka, Hang Tuah Jaya, 76100 Durian Tunggal, Melaka, Malaysia

[2)] Engineering Materials Department, Faculty of Manufacturing Engineering, Universiti Teknikal Malaysia Melaka, Hang Tuah Jaya, 76100 Durian Tunggal, Melaka, Malaysia

[*]Corresponding e-mail: edee@utem.edu.my

Keywords: Oil palm shell, activated carbon, kenaf fiber

ABSTRACT – The application of natural fibers in composite is very encouraging because of its many benefits such as more environmental friendly and cost reduction. The mechanical properties of kenaf fiber reinforced polypropylene composite added with two different types of bio-based fillers, namely oil palm shell powder (OPSP) and activated carbon of oil palm shell powder (ACOPSP) are studied. The composites were prepared by melt mixing of the materials using internal mixer, followed by extrusion and compression molding processes. The samples were prepared at 4 different weight percentage of filler content, i.e., 0, 5, 10 and 15 phc.

1. INTRODUCTION

Natural fiber reinforced composites including kenaf fiber reinforced polypropylene composite have become a potential structural material with many attractive properties such as low density, cost effective, higher deformability and less abrasive. In recent times, kenaf has been used as an alternative to replace wood in pulp and paper industries [1].

Oil palm shell is an industrial waste produced by palm oil industry, which is one of the main sources in Malaysia's economy. Besides producing crude palm oil as the main product, it also produces a million of tonnes of oil palm waste in various forms such as fronds, trunk, empty fruit bunch and shell [2]. Oil palm shell is the shell fractions left after the nut has been removed after crushing in the palm oil mill.

Activated carbon is carbonaceous in nature and exhibit high content of organic substance and in particulate form. It can be produced from biomass and has the potential as alternative sources of fillers. Oil palm shell contains high lignocellulosic fibers and can be used to produce biocarbon (activated carbon) after undergo pyrolysis and carbonization process [3].

2. EXPERIMENTAL

2.1 Materials

Kenaf fibers were in non-woven sheets and supplied by Kenaf Natural Fiber Industries Sdn. Bhd. The oil palm shells were obtained from Jugra Oil Palm Sdn. Bhd. The activated carbon of oil palm shell came in granular form and produced by Standards and Industrial Research Institute of Malaysia (SIRIM). The polypropylene (PP) was purchased from Polypropylene Malaysia Sdn. Bhd. The coupling agent used in this experiment was maleic anhydride grafted polypropylene (MAgPP) and produced by Sigma Aldrich.

2.2 Sample Preparation and Testing

Initially, oil palm shells were cleaned with water and dried under sunlight for 10 hours. To produce the powder of oil palm shell (OPSP) and activated carbon of oil palm shell (ACOPSP), the oil palm shell and its activated carbon aggregates were crushed using crusher and subsequently pulverized by using a variable speed rotor mill (Pulverisette, FRITSCH). The OPSP and ACOPSP particles were then sieved using a vibratory sieve shaker (Analysette, FRITSCH) to obtain particle size of approximately 45 µm. The amounts of OPSP and ACOPSP were varied at 0, 5, 10, 15 per hundred compounds (phc), while the composition of kenaf/PP was fixed at 30/70 wt%. The formulations for the composites are shown in Table 1.

Table 1 Formulations of the OPSP/kenaf/PP and ACOPSP/kenaf/PP composites

Kenaf (wt%)	PP (wt%)	OPSP or ACOPSP (phc)	MAgPP (phc)
30	70	0	3
		5	
		10	
		15	

Fabrication of composite samples was carried out by sandwiching a non-woven kenaf with OPSP/PP or ACOPSP/PP sheets. The sheets were prepared by melt mixing PP and the biomass-derived filler using internal mixer at 180 °C for 10 min, followed by extrusion and lastly, compression moulding for 10 min at 180 °C and 10 MPa. Finally, it was cooled at room temperatures for 10 minutes, before being cut into standard samples.

Tensile and flexural tests were performed using Universal Testing Machine according to ASTM D638 and ASTM D790, respectively. For each composition, the average value for five measurements was taken as the result.

3. RESULTS AND DISCUSSION

The results obtained from the tensile and flexural tests of the composites are shown in Figures 1 – 4. The tensile strength for OPSP composite increased as the filler content added from 0 to 15phc. For the ACOPSP composite, the tensile strength increased at 5phc, but decreased when the filler content was further increased to 10 and 15 phc.

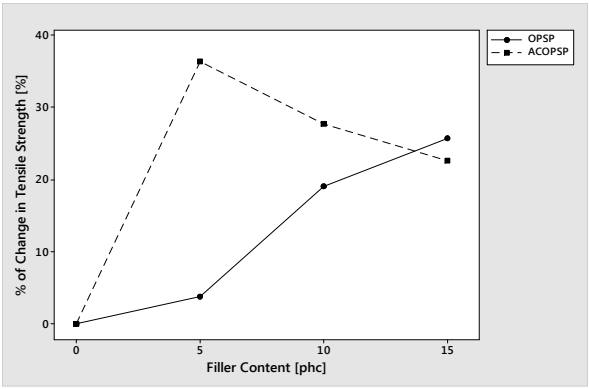

Figure 1 Percentage of change in tensile strength of the OPSP and ACOPSP composites

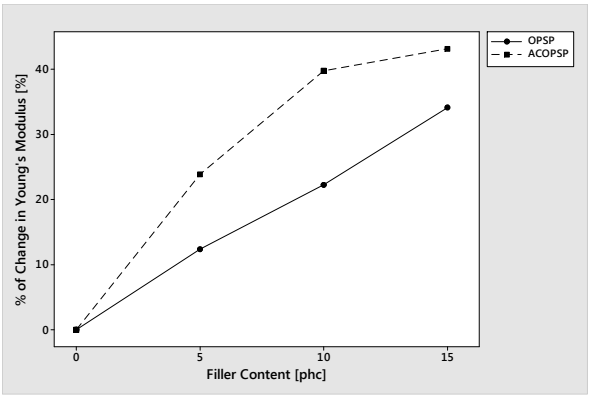

Figure 2 Percentage of change in tensile modulus of the OPSP and ACOPSP composites

The flexural strength shows a similar result to that of tensile strength in which the OPSP composite show a consistent increase in flexural strength with the addition of OPSP filler up to 15 phc, while the ACOPSP composite show a decrease as the filler content is increased above 5 phc. It is suggested that the decrease observed in the composite added with higher content of ACOPSP is possibly due the agglomeration of the ACOPSP filler, which is associated with its higher specific surface area as observed by the SEM analysis.

The Young's and flexural moduli for both composites show a similar trend. There is an improvement of the modulus properties when the composites were added with the biomass fillers from 0 to 15 phc, however the increase is more significant in flexural modulus than tensile modulus.

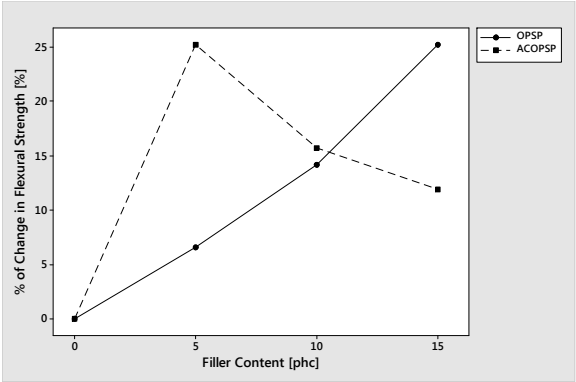

Figure 3 Percentage of change in flexural strength of the OPSP and ACOPSP composites

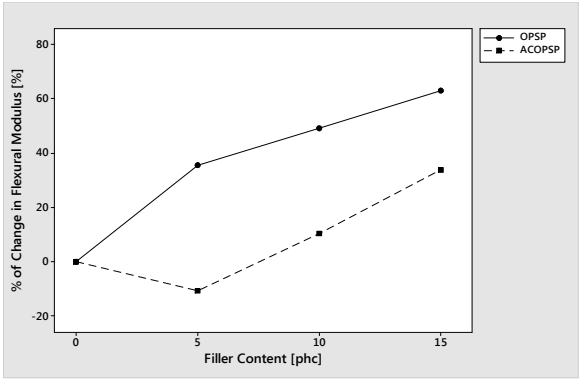

Figure 4 percentage of change in flexural modulus of the OPSP and ACOPSP composites

4. CONCLUSIONS

It can be concluded that the addition of OPSP and ACOPSP fillers to the kenaf/polypropylene composite is effective to improve the mechanical properties of the composite. Both types of composites show a consistent increase in tensile and flexural moduli with the increase of filler content. Meanwhile, only OPSP composite shows a consistent increase in tensile and flexural strength with the increase of OPSP content, but ACOPSP composite started to decrease in those values when then amount of ACOPSP is more than 5 phc.

REFERENCES

[1] O. Faruk, A.K. Bledzki, H.P. Fink, and M. Sain, "Progress report on natural fiber reinforced composites," *Macromolecular Materials and Engineering*, vol. 299, no. 1, pp.9-26, 2014.

[2] H.P.S. Khalil, R.N. Kumar, S.M. Asri, N.A. Nik Fuaad, and M.N. Ahmad, "Hybrid thermoplastic pre-preg oil palm frond fibers (OPF) reinforced in polyester composites," Polymer-*Plastics Technology and Engineering*, vol. 46, no. 1, pp.43-50, 2007.

[3] H.A. Khalil, N.Z. Noriman, M.N. Ahmad, M.M. Ratnam, and N.N. Fuaad, "Polyester composites filled carbon black and activated carbon from bamboo (Gigantochloa scortechinii): Physical and mechanical properties," *Journal of Reinforced Plastics and composites*, vol. 26, no. 3, pp.305-320, 2007.

Proceedings of Innovative Research and Industrial Dialogue'16, pp. 39-40 (May 2017)

Finite element modelling for composites single lap join plate using four elements

A.F. Ab Ghani*, M.B. Ali, M. Ahadlin, N.A.A. Md Zahir

Faculty of Mechanical Engineering, Universiti Teknikal Malaysia Melaka (UTeM), Melaka, Malaysia

*Corresponding e-mail: *ahmadfuad@utem.edu.my

Keywords: Composite FEM, 3D continuum shell, composite lap joint

ABSTRACT – This study is to analyze the finite element modelling for composite single lap join plate by using four different elements which are 2D plane strain, 2D plane stress, 3D conventional shell and 3D continuum shell. With finite element modelling features in ANSYS version 13.0, the accuracy, mesh convergence and reliability of composite have been tested. The study begins with analysis on mesh convergence followed by computation of stress experienced on composite under uniaxial tensile loading. Peak normal stress and shear stress of 3D continuum shell shows significant different at the edge of the overlap joint where stress concentration and point of singularity exist.

1. INTRODUCTION

Performance prediction is an important aspect in confirming the correct design specification of composite materials. General purpose computer programs for finite element analysis emerged in the late 1960's and early 1970's. To ensure correct design specification of composite material, performance prediction plays an important role. This can be done with the aid of finite element method (FEM) to analyze the composite structure under static loading [1]. This approach can be used for more accurate strength prediction in terms of stress and strain components of a structure. 3D model of adhesive joints based on shell and solid elements finite element modelling has been developed to study the effect of different element used in modelling composite material on stress distribution in adhesive joint. The output to measure can be in the form of deformation of material such as deflection, displacement, in plane strain, out of plane deformation etc[2]. In this study, it is aimed to explore the effect of bending which account for normal stress experienced by composite as well as shear effect in the composite material in the mode that represented in composite single lap joint.

2. METHODOLOGY

To simulate the deformation of composite ply in the form of single lap joint, correct boundary conditions are ensured. This was made similar in representation with the real experimental set up where the one end of composite adherend is fixed (as in clamp during experimental) and the other end is moving in uniaxial direction (as in experimental set up at tensile mode). Significant effect of bending can be quantified if two composite materials (adherends) connected together with adhesive (modelled as solid) as compared to a single composite material being applied load at one end and the other end is fixed to observe the deformation [3]. In this study, the effect of bending and shear were observed and noticed in the adhesive layer in the form of normal stress and shear stress along the overlap length.

Figure 1 shows 3D finite element model for composite single lap joint used in this study. This consists of two important parameters which are; boundary condition and coupling of adherend and adhesive. The correct boundary conditions need to be confirmed to simulate the deformation of composite ply.

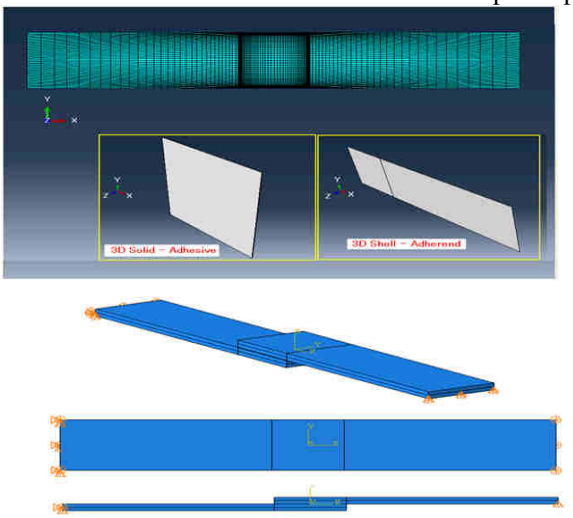

Figure 1 3D FE model for composite single lap joint

Adherend and adhesive are assumed to be perfectly bonded to each other at the overlap surface of the lap joint as shown in Figure 2. Force applied is F=100 kN/m and in 3D continuum model, load applied as pressure load. When T describes the thickness of the adherent, the tensile stress was estimated as 30.769 N/mm2. Unit relationship is KN/m= N/mm.

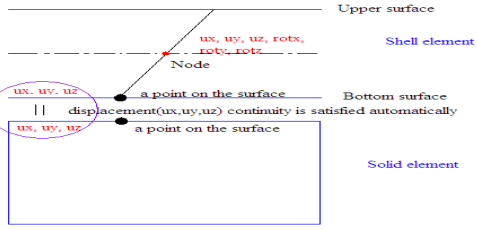

Figure 2 Illustration shows bonded condition at the interface of shell element and solid element [4]

3. RESULTS

For 3D continuum shell, result in Figure 3 shows that deflection in z direction when the joint is deformed under tensile loading. The details of the meshing configurations for adhesive part model and meshing of adherent correspond to 8 elements through thickness and 8 elements across width.

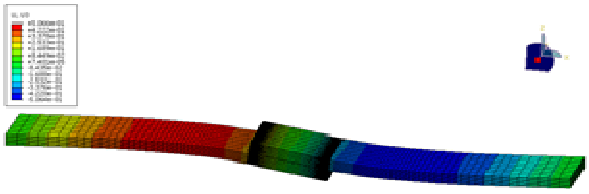

Figure 3 Deflection in Z direction; out of plane direction

Different peak of peel stress was accounted for 4 different elements used to represent the composite adherend and this peek stress was found at the edge of the sharp corner of the joint where highest stress concentration occurred in Figure 4.

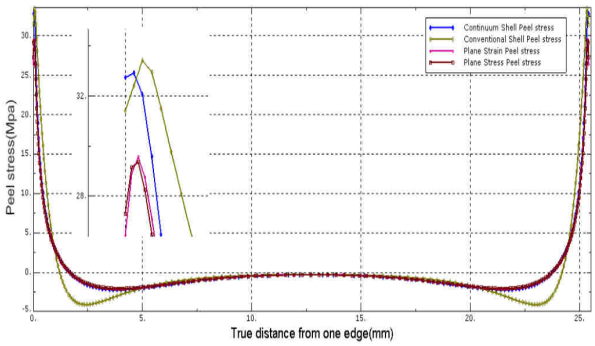

Figure 4 Peel stress plot along the centerline at the adhesive layer

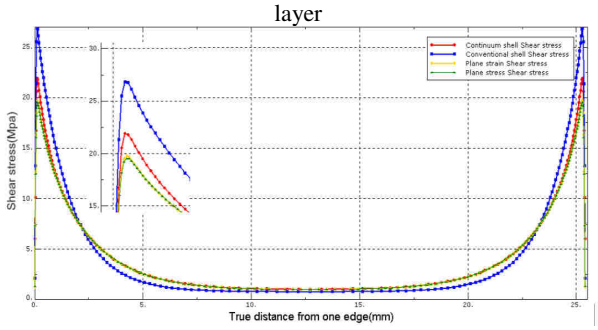

Figure 5 Shear stress plot along the centerline at the adhesive layer

Higher peak stress for peel/normal is shown in plane strain as compared to plane strain condition. Figure 5 shows the similar trend for shear stress computed at the same location on adhesive layer.

4. DISCUSSION

3D continuum shell analysis was done with the simulation for four different elements which are plane strain, plane stress, 3D continuum shell and 3D conventional shell. Parameters such as thickness, composite layup and orientation, material properties remain constant across four types of elements used. Asymmetric mode of deformation on composite adherend and adhesive results in the occurrence of variation of stress along centerline of adhesive layer during deformation of composite single lap joint under tensile loading. Conventional shell accounted slightly higher peel stress and shear stress than continuum shell. In terms of peak shear stress, very slim different is shown by plane strain as compared to plane stress thus reflect that 3D continuum shell to be suitable element for composite. For 2D, value of stress obtained approximately 15 percent different compared to 3D modelling. The width effect, Poisson ratio effect, and transverse shear stress across through thickness all contributed to the discrepancy computed [4, 5].

5. CONCLUSIONS

The study has shown significant output in terms of shear stress and peel stress experienced by adhesive of composite single lap joint based on different element used to represent the composite adherend. The 3D continuum shells performed well than conventional shell and 2D plane stress/plane strain in capturing bending thus the best choice for composite layup.

ACKNOWLEDGEMENT

Authors would like to thanks Universiti Teknikal Malaysia Melaka (UTeM) for ANSYS 13.0 utilization and database for accessing literature. This research is funded under RAGS/1/2015/TK0/UTEM/03/17.

REFERENCES

[1] J.A. Harris, R.D Adams. “Strength prediction of bonded single-lap joints by nonlinear finite element methods”.*International Journal of Adhesion & Adhesives*, vol. 4, pp. 65–78, 1984.

[2] A.T. Nettles. “Basic Mechanics of Laminated Composite Plates,” *NASA Reference Publication* 1351, 1994.

[3] R.H. Andruet, D.A. Dillard, S.M. Holzer, “Two and three dimensional Geometrical nonlinear finite elements for analysis of adhesive joints”, *International Journal of Adhesion and Adhesives*, vol. 21, pp. 17–34. 2001.

[4] ANSYS Mechanical User's Guide 2010

[5] D. Gay and S.V. Hoa, "Composite materials, design and application", *CRC Press*, second edition, 2007.

[6] D. F. Adams, L. A. Carlsson, R. B. Pipes, Experimental Characterization of Advanced Composite Materials, *CRC Press*, 2002.